STIMATE OF THE CLOUDINESS INFLUENCE ON THE EVOLUTION OF RADIATION TEMPERATURE INVERSION IN THE BOUNDARY LAYER OF THE ATMOSPHERE

S.L. Odintsov

Institute of Atmospheric Optics,
Siberian Branch of the Russian Academy of Sciences, Tomsk
Received December 29, 1995

Influence of cloud amount and height of a single-level cloudiness on the formation and evolution of near-ground temperature inversion within the boundary atmospheric layer at night is considered in this paper. Some peculiarities of the inversion height behavior, particularly, its sharp decrease as the cloud amount exceeds certain value are discussed using model estimates. Correlation between the inversion height, cloud amount and dynamic friction velocity is illustrated with model examples.

Many applied problems of atmospheric physics, as well as problems on propagation of waves of different origin in the planetary boundary layer require derivation of efficient algorithms for prediction of short-term variations of the main meteorological parameters within the atmospheric boundary layer (ABL), such as profiles of wind velocity vector, humidity, turbulent fluxes of medium constituents and temperature. It is the temperature among the ABL parameters to be investigated in this paper.

Clearly, the problem on temperature prediction was solved and is solved over tens of years and, therewith, increase in accuracy of ground temperature prediction in the scale range from local to global is generally the main aim of investigations. The question on diurnal behavior of the temperature profile in ABL, along with the inversion distribution of the temperature is less well understood. Nevertheless, such a problem as that on the evolution of radiative temperature inversion under cloudy conditions needs for further analysis. When forecasting temperature profile, cloudiness is generally mentioned as a factor which moderates development of the inversion without specific algorithm of consideration of the cloudiness itself.

The aim of this paper is to close, although partially, this gap in the problem and estimate quantitatively the cloudiness effect on the evolution of radiative ground temperature inversion. In our calculations, the simplest model of evolution of absolute temperature profile $T(z, t)$ with the presence of vertical turbulent heat transfer and radiation cooling of the atmosphere being uniform in the horizontal direction, without considering air advection, is chosen. This model is described by the following expression:

$$\frac{\partial\theta(z, t)}{\partial t} = \frac{\partial}{\partial z}\left[k_T(z, t)\,\frac{\partial\theta(z, t)}{\partial t}\right] + \frac{1}{c_p\rho}\,\frac{\partial R(z, t)}{\partial z}, \qquad (1)$$

Here $\theta(z, t) \approx T(z, t) + 0.01z$ is the potential temperature of air (K), $k_T(z, t)$ is the turbulent thermal diffusivity (m^2/s), $R(z, t)$ is the effective flux of IR radiation at a height z at a time t (W/m^2), $c_p = 1006$ J/(kg·K)·is the air specific heat at a constant pressure, ρ is the air density (kg/m^3). Note that most of the equations used in this paper are taken from Refs. 1 and 2.

Boundary conditions for the equation (1) at $z = 0$ is often based on the following equation of heat balance of the underlying surface:

$$R(0, t) + c_p\,\rho\,k_T(0, t)\,\frac{\partial\theta(0, t)}{\partial z} - \lambda_s\,\frac{\partial T_s(0, t)}{\partial z} + \\ + L_s\,\rho k_T(0, t)\,\frac{\partial w(0, t)}{\partial z} = 0. \qquad (2)$$

Here L_s is the specific heat of water evaporation ($L_s = 2.45$ J/kg at $T(0, t) = 293$ K), $w(0, t)$ is the specific air humidity (kg/kg), λ_s and T_s are molecular heat conductivity and absolute temperature of soil, respectively.

The height of the model upper boundary is defined by either the height of the lower boundary of cloudiness z_c or some height z_T providing reasonably complete consideration of the descending flux of IR radiation under clear sky condition. Boundary condition for the equation (1) at the upper model boundary under clear sky conditions is given by the following expression:

$$\frac{\partial\theta(z_T, t)}{\partial z} = \text{const} \qquad (3)$$

0235-6880/96/07 645-06 $02.00

and is characterized by nonzero absolute temperature with a constant gradient.

Consideration of the cloudiness influence is carried out based on the simplest model: a single-level cloudiness with smooth lower boundary and emissivity being similar to that of a black body. Overcastting range is defined by the cloud amount $N = 0–1$. The second boundary condition for the equation (1) with cloudiness depends on the height of clouds and is described by the equation of the type (3).

Effective flux of IR radiation is defined by the following expression:

$$R(z, t) = G(z, t) - U(z, t), \quad (4)$$

where $G(z, t)$ and $U(z, t)$ are profiles of descending and ascending fluxes of thermal radiation (W/m^2), respectively. These profiles are given by the following equations:

$$G(z, t) = B(z_T, t)D(z, z_T) - \int_z^{z_T} B(z', t)\mathrm{d}D(z, z'), \quad (5)$$

$$U(z, t) = \delta B(0, t)D(0, z) + \int_0^z B(z', t)\mathrm{d}D(z', z) -$$

$$- (1 - \delta)\int_0^z B(z', t)\,\mathrm{d}D[m(0, z') + m(0, z)]. \quad (6)$$

Here δ is the relative absorption coefficient of the Earth's surface, $B(z, t) = \sigma T^4(z, t)$ is the natural emission of the atmosphere (W/m^2), $\sigma = 5.67\cdot10^{-8}$ W/m^2K^4 is the Stefan-Boltsman constant, $D(z_1, z_2)$ is the diffuse integral function of the atmospheric transmittance (only water vapor is considered), $m(z_1, z_2)$ is a function of the water vapor mass in the air column with a unit area between z_1 and z_2 heights. The function $D(z_1, z_2)$ is taken in the following form (see Ref. 3):

$$D(z_1, z_2) = 0.74e^{-0.28\,\varkappa} + 0.26e^{-5.5\,\varkappa}, \quad (7)$$

where

$$\varkappa = m/\sqrt{m + 0.0001};\ m(z_1, z_2) = 1.67\int_{z_1}^{z_2} \rho_w(z')\mathrm{d}z';$$

$\rho_w(z)$ is the density of water vapor. The radiative inflow (sink) of heat in ABL governed by the second term in the right-hand side of Eq. (1) is calculated based on Eqs. (4)–(7).

The radiative balance of the underlying surface under cloudy conditions is given by the following expression:

$$R(0, t) = N\,R_1(0, t) + (1 - N)R_0(0, t), \quad (8)$$

where R_1 and R_0 are the radiative balances of the underlying surface at an overcast and clear sky, respectively, N is the cloud amount.

The main factor that governs the temperature profile dynamics in the ABL is turbulent heat flux whose parametrization causes the need for simulation of the turbulent thermal diffusivity $k_T(z, t)$. Many papers have been devoted to solution of this problem (see, for example, Refs. 8 and 9 and references therein). However, no versatile model of $k_T(z, t)$ has been constructed yet. Therefore, when simulating $k_T(z, t)$ either empirical equations resulting from local experiments or expressions following from a set of theoretical grounds are used. In this paper, a model of k_T is proposed based on the results from Refs. 4 and 5

$$k_T(z, t) = \begin{cases} k_0 + \alpha\varkappa_K\, u_*\, z/\varphi(z, t), & z \le h(t), \\ k_a + k_T(h)\exp(-\beta[z - h(t)]), & z > h(t), \end{cases} \quad (9)$$

$$\varphi(z, t) = \begin{cases} 1 + 6.34\xi, & 0 < \xi \le 1, \\ 7.34, & 1 < \xi. \end{cases} \quad (10)$$

Here $k_0 = 1.4\cdot10^{-5}$ m^2/s is the molecular air thermal diffusivity, k_a is turbulent thermal diffusivity above the inversion, $\varkappa_K = 0.4$ is Karman constant, u_* is the dynamic friction speed, $\alpha = 1.35$, parameter β controls the fall-off rate of $k_T(z, t)$ in the region above the main turbulized layer at a height $h(t)$, $\xi = z/L(t)$ is the dimensionless height, $g = 9.81$ m/s^2, $L(t) = -u_*^3\, c_p\, \rho T(0, t)/\varkappa_K\, g\, Q_T(t)$ is Monin-Obukhov scale, $Q_T = -c_p\, \rho k_T(0, t)\partial\theta(0, t)/\partial z$ is the turbulent heat flux at the underlying surface. The conditions to be considered in this paper are characterized, in particular, by $Q_T \le 0$. Hence, the scale L is above zero. In this case, the height of turbulized layer, $h(t)$, can be written as

$$h(t) = \frac{0.3u_*}{f\left(1 + (0.353/\varkappa_K)\sqrt{u_*\,\varkappa_K/fL(t)}\right)}. \quad (11)$$

Here $f = 2\omega\sin\Omega$ is the Coriolis parameter for the latitude Ω, $\omega = 7\cdot10^{-5}$ rad/s is the angular speed of the Earth's rotation.

Thus, we have practically defined the functions and the parameters which are necessary for solving Eq. (1) with the boundary conditions (2) and (3). So we have now to propose a model of latent heat fluxes and heat flux from the soil deep. Comprehensive estimation of those fluxes is possible based on the solution of a set of corresponding differential equations including Eq. (1). In this case, the state of the ground air layers, plant cover and soil interacting with each other is extremely variable. Therefore, taking into account the idea of the problem to be formulated in this paper, there is a little point to simulate such specific conditions. In accordance with this assumption, the condition for latent heat fluxes and heat flux from the soil deep were assumed to be connected with the radiative balance and have the value $W\cdot R$, where $W < 1$. That is, the following expression is valid

$$-L_s\rho k_T(0, t)\frac{\partial w(0, t)}{\partial z} + \lambda_s\frac{\partial T_s(0, t)}{\partial z} = WR(0, t). \quad (12)$$

This equation reduces the boundary condition (2) to the following form:

$$(1 - W)R(0, t) + c_p\,\rho k_T(0, t)\frac{\partial\theta(0, t)}{\partial z} = 0. \quad (13)$$

The variations of W provide a simplified consideration of effects of latent fluxes and heat fluxes from the soil on the heat balance of the underlying surface.

Numerical method of finite differences was used to solve Eq. (1). The finite-difference model (FDM) with a nonuniform grid in time and height (see Ref. 7) was taken as a basis for calculations. Specifically, the monotonic Krank–Nicholson schematic model with a unity weight on a six-point two-layer template was realized. Stability of the solution is achieved by following the selection rules of the initial model parameters, proposed in Ref. 7. The developed finite-difference algorithm for solution for Eq. (1) was tested by its analytical solutions resulting from sufficient simplification of the functions entering into the equation and its boundary conditions.

When employing the FDM, estimations of advance values of the source function [second term in the right-hand side of Eq. (1)] and radiation balance of the Earth's surface dependent on temperature are needed. For this purpose, the temperature profile from the preceding time step is used in our calculations. Of course, this introduces certain errors into the forecast, but these errors are insufficient to violate the temperature profile to be predicted. This conclusion was tested both by analytically solved models and by changing parameters in the finite-difference schematic model. Note also that finite differences were not used everywhere over the height region $0 \le z \le z_T$. Below this point will be discussed in a more detail.

Before considering the calculational results, let us mention the main parameters of the computation model and insert them into a "standardB set. Only deviations from this set will be noted below. The values of the parameters from the set were chosen irrespective of the specific situation. Then, let us set the initial structure of the temperature profile and assume that at clear sky the upper boundary in the model $z_T = 25$ km and absolute temperature profile above $z_u = 2$ km varies according to the following model:

$$T(z) = \begin{cases} T(z_u) - 6.5(11 - z_u), & z_u < z \le 11\ \text{km}, \\ T(z = 11\ \text{km}), & 11\ \text{km} < z \le z_T. \end{cases} \quad (14)$$

Solution of the Eq. (1) was combined from the solutions for the layers in the following ranges of z: $z_u \ge z \ge z_l$ (z_l =1 km) and $z_l > z \ge 0$. The condition proposed for the first range is

$$\theta(z, t) = T(z_l, t) + 0.01z_l = \text{const}, \quad (15)$$

which estimates $\partial\theta(z, t)/\partial z = 0$ at $z_u \ge z \ge z_l$ (that is, potential temperature is fixed with height, but it can vary in time). Fulfillment of this condition is achieved, firstly, by the model of the coefficient $k_T(z, t)$, which rapidly approaches a constant value $k_T = k_a$ above $h(t)$ and, secondly, by the assumption that radiative cooling of the atmosphere is independent of height starting with some level $z_r \le z_l$. Certainly, this assumption introduces errors into $T(z, t)$ profile to be predicted. But, as the test calculations show, these errors are not significant for those temperature distributions which are presented in the below examples. As a result, radiative cooling of the atmosphere independent of height occurs in the layer with $z \ge z_l$. Equation (1) is numerically solved for the atmospheric layer with $0 \le z \le z_l$ using finite-difference schematic model whose boundary conditions are defined by the expression (13) for the boundary $z = 0$ and by the equation $\partial\theta/\partial z = 0$ at the height $z = z_l$ which serves as the second boundary of the FDM. Note once more that the temperature profile model presented above is determined for the cloudless conditions. Under cloudy conditions with the lower boundary of clouds at $z_c \le z_l$, calculations from finite differences are performed for all layers below the clouds. Otherwise, "two-layerB solution is used. The profile of water vapor density in our calculations obeys the condition of constant behavior of relative humidity U_0 with height.

For the term "cloudlessB to be completely defined, we give the values of the above-mentioned parameters used in our calculations: $u_* = 0.15$ m/s, $\beta = 0.01$, $\Omega = 56°$N, $\delta = 0.986$, $z_r = 800$ m, $k_a = 0.005$ m^2/s, $u_0 = 70\%$, $W = 0.8$. Under cloudy conditions, values $N = 1$ and $z_c = 5000$ m must be added to this set of parameters to describe the term "cloudyB (overcast with its lower boundary at 5 km). The initial temperature profile in the layer with $0 \le z \le z_l$ is assumed to fit the indifferent stratification, that is, $\partial\theta(z, 0)/\partial z = 0$ at $T(0, 0) = 293$ K and $T(z, 0) = T(0, 0) - 0.01z$. The model temperature profile for high atmospheric layers has been preset earlier.

Coming to calculational results, we would like to note first of all the order of values describing specific processes and parameters. Thus, Fig. 1*a* depicts variations of air temperature profile over period from 21 p.m. of local time to 6 a.m. of the next day for cloudless (solid lines) and cloudy (dashed line) conditions at the same initial profile $T(z, 0)$. It is evident that cloudiness with cloud amount less than unity will result in changes of the temperature profile. Moreover, the plot of these changes will be placed between solid and dashed lines *2*. The heat fluxes Q_T under cloudless and cloudy conditions vary in the ranges from -20 W/m^2 and -11 W/m^2 at the beginning of the forecast to -15 W/m^2 and -8 W/m^2 by its end, respectively. Remind that the equation $Q_T(t) = (1 - W)R(0, t)$ is valid in the given model. Moderate overnight changes in Q_T and temperature of underlying surface at "standardB conditions produce only small-scale changes in the height of turbulized layer $h(t)$ (from 69 to 76 m for cloudless conditions

and from 89 to 97 m for the cloudy ones, respectively). Small-scale changes in turbulent thermal diffusivity are also evident (see Fig. 1*b*). Moreover, turbulent heat exchange is faster under cloudy conditions.

Radiative heat sinks above several meters from the surface at the initial time are (−0.15 – −0.25)K/h at clear sky and (−0.05 – −0.1)K/h under cloudy conditions. Radiative cooling in the ground layer sharply increases and peaks at $z = 0$. Its maximum values equal −11.5K/h and −6.1K/h under cloudless and cloudy conditions, respectively. By the end of the time interval considered, the rate of radiative cooling considerably changes only in the lower part of the ABL. In this case the rate of surface cooling at the expense of this process is (−5 – −4)K/h and the profile takes the shape characteristic of the inversion conditions (see Fig. 1*c*).

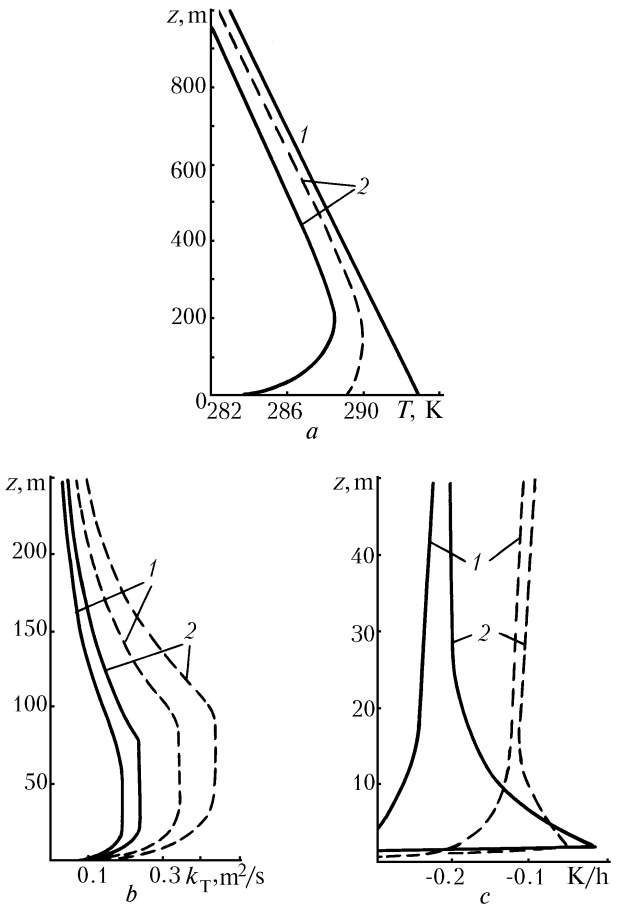

FIG.1. Example of absolute temperature (a), turbulent thermal diffusivity (b) and radiative cooling rate (c) profiles under cloudless (solid lines) and cloudy (dashed lines) conditions. Curves 1 and 2 correspond to the initial and finite points of time, respectively.

It should also be mentioned that the temperature profile model limited by the height $z_T = 25$ km with non-zero temperature at that height slightly underestimates the atmospheric radiative cooling (by about −0.05K/h in ABL). However, such an error is no more than that due to simplification of different processes and can be neglected.

Let us now examine the effect of cloudiness itself on the inversion evolution. In so doing, only the height of the inversion H_{in} and the temperature difference ΔT_{in} across the inversion layer will be considered instead of the profiles themselves thus providing a decrease in the graphical data to be presented. Unfortunately, in this case visual demonstration of the process of $T(z, t)$ transformation will be poorer. Application of finite-difference schematic model provides discrete, with height, values of the desired parameters. Approximation of the temperature profile by a polynomial in data processing allows us to find estimations of the inversion height in the case when the height is between the grid nodes.

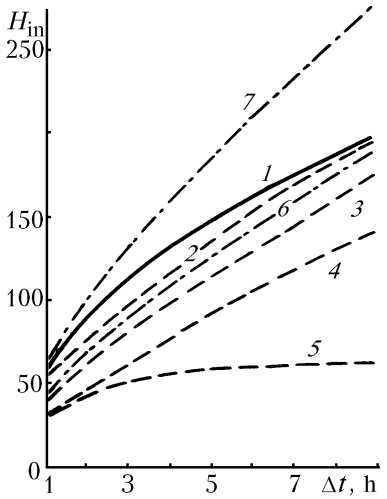

FIG. 2. Inversion height as a function of cooling time under cloudless (curve 1) and overcast conditions (dashed lines). Curves 2, 3, 4, and 5 correspond to z_c = 10, 7, 5, and 3 km, respectively. For comparison, the empirical curves[8] at weak (6) and moderate (7) wind are presented

First of all, we consider time dependence of the inversion height at clear sky and at overcast with different height of its lower boundary. Figure 2 depicts H_{in} as a function of forecast period $\Delta t = t - t_0$ (here the forecast is assumed to start at 6 p.m. of local time when the darkness comes). Solid and dashed lines correspond to clear sky and cloudy conditions, respectively. Two curves (dot-and-dash lines) from Ref. 8 are presented here, as well. These curves correspond to experimental data obtained at low (curve *6*) and moderate (curve *7*) wind from high-altitude tower measurements in Obninsk. Quantitative estimations of cloudiness over the period of measurements are not presented in Ref. 8. The inversion depth ΔT_{in} from the model calculations depicted in Fig. 2 peaks by the end of the forecast and comprises 4.5 K at clear sky with $z_c = 5$ km and 0.5 K at cloudy conditions with $z_c = 3$ km, respectively. Comparison

between ΔT_{in} values and those obtained from empirical expression,[8] $\Delta T_{in\,e} = q[T(0, 0) - T(0, \Delta t)]$, $q = 0.65 \pm 0.12$, gives the following results. Value of $\Delta T_{in\,e} = (5.8 \pm 1.1)$K correlates with that of ΔT_{in} under cloudless conditions, but $\Delta T_{in\,e}$ differs significantly from ΔT_{in} under cloudy conditions. For example, $\Delta T_{in\,e}$ value as high as (2.6±0.48)K takes place under cloudy conditions ($z_c = 5$ km, $N = 1.0$). Note that a set of parameters, including cloud amount, to be used in calculations should be well agreed for a proper comparison of simulated and calculated values of the inversion depth. Nevertheless, it is reasonable to assume that model calculations as a whole take an equivalent account of the main processes of the inversion formation and they can be used for estimation of the cloudiness effect on the evolution of temperature field in ABL.

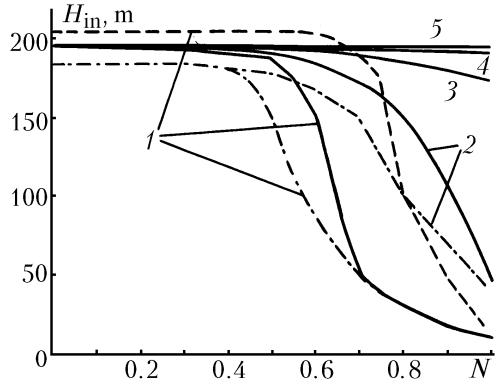

FIG. 3. Inversion height versus cloud amount and cloudiness height. Curves plotted by solid, dashed, and dot-and-dash lines are obtained at a standard set of parameters, $W = 0.7$, and $\delta = 1$, respectively. Curves 1, 2, 3, 4, and 5 correspond to cloudiness height of 1, 3, 5, 7, *and* 10 km, *respectively.*

The calculations performed make it possible to show a number of plots demonstrating height of inversion as functions of cloud amount and height of cloudiness lower boundary to be constructed. Thus, Fig. 3 depicts H_{in} versus z_c and N after nine-hour evolution. Behavior of H_{in} at low cloudiness and high cloud amount is most interesting, namely, sharp decrease of the inversion height as cloud amount exceeds some critical value. Actually, there is a threshold value of N, exceeding which at a given height of cloudiness practically ensures the absence of inversion in the ABL since the inversion depth under these conditions is only several tenths degree. Clearly, deviations from standard conditions could result in displacement of the threshold value. For example, dependences for $W = 0.7$ (dashed line) and for $\delta = 1.0$ (dot-and-dash line) are also shown in Fig. 3. Displacement of the threshold value of N is apparent.

Neglect of the temperature advection in Eq. (1) does not preclude consideration of the wind action on such an important parameter as turbulent thermal diffusivity $k_T(z, t)$. This is achieved by varying the dynamic velocity u_* which enters into both the equation for k_T and the expression for the turbulized layer height inside the inversion, $h(t)$. It is well known that the higher is the wind, the higher is u_*. It is also a fact that if clouds are observed, the wind occurs. Therewith, as a rule, the lower cloudiness, the higher wind. Based on these facts, we consider the relationship between wind, cloudiness and inversion height in the simplest approximation. On the basis of data presented in Ref. 1, let us assume that at clear sky calm conditions $u_* = 0.05$ m/s, whereas under cloudy conditions dynamic velocity is given according to Table I.

As our calculations show, dynamic friction velocity has a strong effect on the inversion formation. Initial increase of height H_{in} with cloud amount increase and its rather sharp decrease as the cloud amount exceeds some value are shown in Fig. 4.

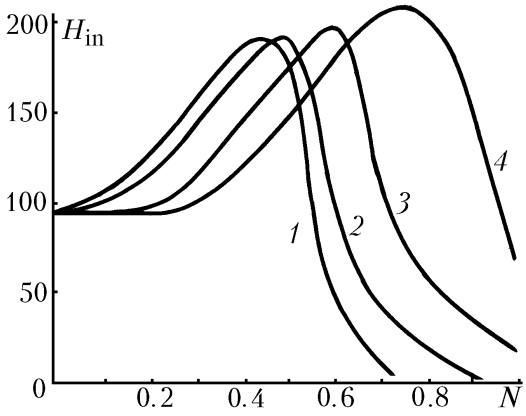

FIG. 4. Inversion height versus cloud amount and cloudiness height after nine-hour cooling of the underlying surface. Certain value of the dynamic friction velocity listed in Table I corresponds to certain cloud amount and cloudiness height values. Curves 1, 2, 3, and 4 correspond to cloudiness height of 3, 5, 7, *and* 10 km, *respectively.*

The physical grounds for this are very simply, i.e., the higher is the value of the coefficient $k_T(z, t)$, the faster comes the process of smoothing temperature inhomogeneities and the process of heat exchange between layers involves higher layers of the ABL. Thus, if the rate of radiative cooling of the underlying surface is less or equal to the rate of turbulent heat inflow from the atmosphere, the inversion does not occur. Therefore, if radiative cooling of soil dominates over heat inflow from both soil and the atmosphere, formation of the inversion starts. In this case, the faster is the ground temperature fall and the higher is the turbulent thermal diffusivity, the higher is the inversion height. Cloud amount controls IR radiation fluxes, while dynamic velocity controls turbulent heat exchange. These are just the parameters whose balance determines the height of the resultant

inversion. As to the curves presented in Fig. 4, the following statement can be made. The range of conditions, where cooling of underlying surface dominates, is located to the left of the curve maximum, whereas turbulent heat exchange over the entire height of ABL prevails to the right of the maximum.

TABLE I. Dynamic velocity, m/s.

Height,	cloud amount, N								
z, km	0.2	0.3	0.4	0.5	0.6	0.7	0.8	0.9	1.0
10	0.05	0.05	0.08	0.10	0.13	0.15	0.17	0.19	0.20
7	0.05	0.07	0.10	0.12	0.15	0.18	0.20	0.21	0.22
5	0.07	0.10	0.12	0.15	0.18	0.20	0.22	0.24	0.25
3	0.10	0.12	0.15	0.17	0.20	0.22	0.25	0.27	0.28

In conclusion, we emphasize once more that the data presented in this paper have been obtained from the simplest model of heat exchange between air and soil. Reliable quantitative data can be found only from an extended simulation of conditions and processes involved in the inversion formation in ABL including consideration of the radiative transfer under conditions of broken clouds.

REFERENCES

1. L.T. Matveev, *Course of General Meteorology. Physics of the Atmosphere* (Gidrometeoizdat, Leningrad, 1976), 640 pp.
2. P.N. Belov, E.P. Borisenkov, and B.D. Panin, *Numerical Methods of Weather Forecast* (Gidrometeoizdat, Leningrad, 1989), 376 pp.
3. M.G.Evseeva, V.E. Mikhailova, E.L. Podol'skaya, and V.G. Tereshchenko, Trudy LGMI, No. 49, 143–158 (1974).
4. A.L. Kazakov and G.L. Lazriev, Izv. Akad. Nauk SSSR, Fiz. Atmos. Okeana **14**, No. 3, 257–265 (1978).
5. I.N. Kuznetsova, Trudy Gidromettsentra SSSR **308**, 68–75 (1990).
6. S.S. Zilitinkevich, E.E. Fedorovich, and M.V. Shabalova, Izv. Akad. Nauk SSSR, Fiz. Atmos. Okeana **27**, No. 4, 339–352 (1991).
7. A.A. Samarskii, *Theory of Difference Schemes* (Nauka, Moscow, 1989), 616 pp.
8. N.L. Byzova, V.N. Ivanov, and E.K. Garger, *Turbulence in the Boundary Atmospheric Layer* (Gidrometeoizdat, Leningrad, 1989), 264 pp.
9. F.T.M. Newstadt and H. Van Dop, eds., *Atmospheric Turbulence and Admixture Dispersal Modeling* (Gidrometeoizdat, Leningrad, 1985), 352 pp.